Calcium transport into the cells of the sea urchin larva in relation to spicule formation

Netta Vidavsky[a], Sefi Addadi[b], Andreas Schertel[c], David Ben-Ezra[d], Muki Shpigel[d], Lia Addadi[a], and Steve Weiner[a,1]

[a]Department of Structural Biology, Weizmann Institute of Science, 76100 Rehovot, Israel; [b]Life Sciences Core Facilities, Weizmann Institute of Science, 76100 Rehovot, Israel; [c]Global Applications Support, Carl Zeiss Microscopy GmbH, 73447 Oberkochen, Germany; and [d]Israel Oceanographic and Limnological Research, National Center for Mariculture, Eilat 88112, Israel

Edited by Paul G. Falkowski, Rutgers, The State University of New Jersey, New Brunswick, NJ, and approved September 30, 2016 (received for review July 21, 2016)

We investigated the manner in which the sea urchin larva takes up calcium from its body cavity into the primary mesenchymal cells (PMCs) that are responsible for spicule formation. We used the membrane-impermeable fluorescent dye calcein and alexa-dextran, with or without a calcium channel inhibitor, and imaged the larvae in vivo with selective-plane illumination microscopy. Both fluorescent molecules are taken up from the body cavity into the PMCs and ectoderm cells, where the two labels are predominantly colocalized in particles, whereas the calcium-binding calcein label is mainly excluded from the endoderm and is concentrated in the spicules. The presence of vesicles and vacuoles inside the PMCs that have openings through the plasma membrane directly to the body cavity was documented using high-resolution cryo-focused ion beam-SEM serial imaging. Some of the vesicles and vacuoles are interconnected to form large networks. We suggest that these vacuolar networks are involved in direct sea water uptake. We conclude that the calcium pathway from the body cavity into cells involves nonspecific endocytosis of sea water with its calcium.

SPIM imaging | endocytosis | in vivo imaging | biomineralization | cryo-FIB-SEM

Ions destined for skeletal formation are sequestered from the environment and are then transported to the cells responsible for mineralization. Food and/or the aqueous medium in which the organism lives are the sources of ions (1–5). The ion transport pathways can be complex and involve cells with specific channels and/or pumps in their membranes, direct communication between cells, transport into vesicles within cells, into cavities with body fluids and, in the case of certain animals, transport through the vasculature (1, 4–9). The ions are often concentrated inside vesicles where they precipitate to form highly disordered mineral phases (10–14). Intracellular mineral-bearing vesicles are also present in other cells where they presumably fulfill functions such as ion reservoirs for various metabolic functions, and for detoxification (15–17). There is some evidence in bone formation that the intracellular mineral is transferred as such to the extracellular space by what seems to be exocytosis (11). Here we investigate the transport of calcium ions from the larval sea urchin body cavity (blastocoel) into the primary mesenchymal cells (PMCs) responsible for spicule formation, where some of these ions are stored as an amorphous calcium carbonate phase inside vesicles (10).

Selective ion uptake into cells involves passage across the cell membrane through ion channels or pumps. Ion channels are induced to open by voltage or ligand binding, selectively allowing ions to diffuse along concentration gradients (18, 19). Ion pumps require energy and actively transfer ions across the cell membrane against the concentration gradient. A nonselective means of ion transport into cells is endocytosis. During endocytosis the plasma membrane deforms and captures extracellular material, which is transferred into the cell within a membrane-delineated volume (vesicle) (20). There is one documented case in the field of biomineralization, the foraminifera, where sea water is endocytosed and then the so-called sea water vacuoles are transported directly to the site of calcite shell formation (2).

In the sea urchin larva, sea water passively penetrates into the blastocoel. The pH of the body fluids inside the blastocoel is the same as the pH of sea water (21). The PMCs are responsible for spicule formation (22, 23) and both epithelial and mesenchymal cells produce mineral-containing vesicles (10, 24). Mineral-containing vesicles are also present inside a branched filopodial network. The vesicles rapidly move inside the filopodial network and most likely take part in vesicle transport throughout the larva (25). The intracellular vesicles contain amorphous calcium carbonate, which is induced to crystallize after the vesicles are translocated from PMCs into the spicule compartment (6, 10). Here we specifically investigate how calcium ions are transported from the blastocoel to the PMCs.

Studies of the calcium pathways in PMCs show that calcium channel blocking interferes with, but does not eliminate, spicule deposition (26, 27), implying that one calcium pathway toward the spicule must be through the cells (23, 28). Calcium channel blockers are assumed to block the entry of extracellular calcium into the cells (23, 27). Calcein is a fluorescent calcium-binding dye that does not permeate through membranes, channels, or pumps. Calcein was shown to enter the PMCs and label intracellular calcium and the spicules (22, 24, 25, 28, 29). In a correlative study, it was shown that calcein labeling does faithfully track calcium distributions (24), and this is assumed to be the case in the study presented here. The calcium channel blocking experiments, as well as the calcein labeling experiments, therefore show that there are at least two different pathways whereby calcium enters into the PMCs.

Significance

A major challenge in biomineralization is to determine the pathways by which calcium is transferred from external sources to the mineralization site. Using the membrane-impermeable calcium-binding dye calcein and fluorescent dextran, in conjunction or not with a calcium channel blocker, we show that both molecules readily enter the body cavity of sea urchin larvae and the cells responsible for skeleton formation. The documented existence of vesicles in these cells that form openings to the body cavity supports the notion that a major calcium uptake pathway involves direct incorporation of sea water into the cells by endocytosis. This pathway, if proven to be widespread among organisms of other phyla, would radically change our understanding of calcium transport in biomineralization.

Author contributions: N.V., L.A., and S.W. designed research; N.V., S.A., and A.S. performed research; S.A., A.S., D.B.-E., and M.S. contributed new reagents/analytic tools; N.V., L.A., and S.W. analyzed data; and N.V., L.A., and S.W. wrote the paper.

The authors declare no conflict of interest.

This article is a PNAS Direct Submission.

[1]To whom correspondence should be addressed. Email: steve.weiner@weizmann.ac.il.

This article contains supporting information online at www.pnas.org/lookup/suppl/doi:10.1073/pnas.1612017113/-/DCSupplemental.

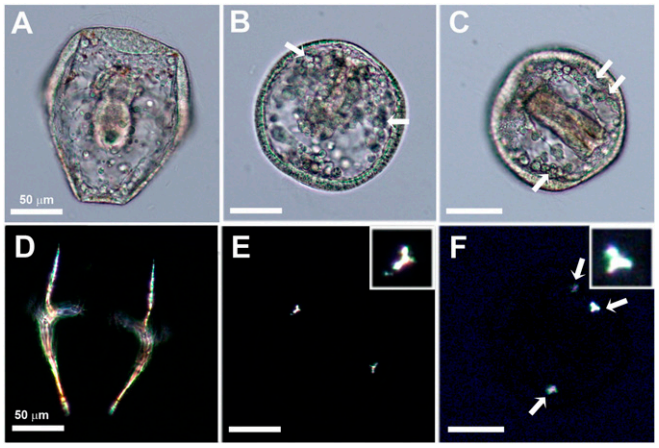

Fig. 1. Light microscope images of living sea urchin larvae 40 h post-fertilization. (*A* and *D*) Sea urchin larva at the prism stage continuously developed inside sea water. The larva has a conical shape at this stage. The spicules are birefringent and appear illuminated under cross-polarizers (*D*). (*B*, *C*, *E*, and *F*) Sea urchin larvae that were continuously developed in the presence of verapamil, which inhibits L-calcium channels. The larvae are developed, showing epithelial layers and the forming gut, but have poorly developed spicules and a spherical shape. Small crystals in the shape of triradiate spicules are observed under polarized light (*E* and *F*). (*B* and *C*) The locations in which the birefringent crystals appear under polarized light are marked with arrows. In *C* and *F* an additional third crystalline granule appears (arrows). *E* and *F*, *Insets* show the magnified triradiate crystals (inset dimensions: 18 × 18 μm). (Scale bars: 50 μm.)

Here we study the consequences of calcium L-type channel inhibition on spicule formation and monitor the processes involved in cellular ion uptake from the environment using calcein and a fluorescent-tagged dextran molecule. One possible transport mechanism is identified by using cryo-focused ion beam (FIB)-SEM serial imaging to obtain high-resolution 3D reconstructions of the blastocoel and PMCs.

Results

Paracentrotus lividus sea urchin larvae reach the prism stage at 40 h postfertilization. When observed under the light microscope, the ectoderm, endoderm, and mesenchymal cells can be easily distinguished at this stage, and filopodial extensions are observed inside the larval body cavity (blastocoel). The larva has a cone-like shape, supported by two well-developed spicules (Fig. 1*A*). The spicules are composed of single crystals of calcite that are birefringent and easily recognized under cross-polarized light (Fig. 1*D*).

The influence of calcium channel inhibition on spicule deposition was studied by growing the larvae in sea water containing the calcium antagonist verapamil for 40 h. Verapamil is an L-type calcium channel blocker (30–32). Verapamil was chosen because during the period of early development of sea urchin larvae $^{45}Ca^{2+}$ uptake and spicule formation are inhibited by verapamil (26, 33). The ectoderm cells and the endoderm cells of the forming gut are clearly visible in the larvae grown with the inhibitor, as they are in larvae grown without the inhibitor. Characteristic mesenchymal cells and filopodial extensions are also observed (Fig. 1*C*). However, the shapes of the larvae are spherical rather than conical (Fig. 1 *B* and *C*) and their spicules are poorly developed. Instead of the well-formed spicules that form in the control larvae at this stage, under Ca-channel inhibition micrometer-size crystalline deposits in the shape of granules or triradiate spicules are seen under polarized light (Fig. 1 *E* and *F*). In some larvae more than two deposits are observed (Fig. 1*F*). Calcium channel inhibition therefore only partially influences mineral deposition, and we conclude that spicule deposition is not entirely dependent on L-calcium channels.

To further elucidate the calcium pathway through the PMCs toward the spicule, calcium was labeled with the fluorescent Ca-chelator calcein (excitation λ = 495 μm, emission λ = 515 μm, green) (22, 24, 25, 28). A 3D view of the calcein distributions inside the larva was obtained by using in vivo selective-plane illumination microscopy (SPIM) with a Lightsheet microscope (*Materials and Methods*). SPIM imaging enables rapid acquisition of fluorescence emission from large volumes (namely the entire larva, which is more than 100 μm^3) with spatial distances between the acquired images of <0.5 μm. This yields a high-resolution reconstruction in 3D. During imaging, the samples suffer minimal bleaching of the fluorescence.

Larvae were grown continuously from fertilization inside calcein-labeled sea water. The calcein label was observed in particles and in the spicules (Fig. 2*A*). It was previously shown by correlative fluorescence microscopy, energy-dispersive X-ray spectroscopy, and Raman spectroscopy that the calcein-labeled particles observed in the sea urchin larvae are composed of calcium mineral (24, 25). From their locations and distribution we infer that the calcein-labeled particles observed with the Lightsheet microscope are mostly intracellular. Higher-intensity calcein labeling appears at the location of the initial crystalline spicule deposit (the precise location was determined from the reconstructed data in 3D), relative to other parts of the spicule (Fig. 2*A*).

The Lightsheet was also used to examine the effect of verapamil on calcein distribution after 40 h. Intracellular calcein-labeled particles are visible all over the larva, together with larger bodies, which are most likely the triradiate spicule rudiments observed under polarized light (Fig. 2*B*). The intracellular particles of the larvae grown with the inhibitor were larger compared with the control larvae. We conclude that in both normal development and under L-type calcium channel inhibition calcein still enters the cells, even though calcein is membrane-impermeable and cannot be transferred through calcium channels together with the calcium ions. This raises the question of how the calcein enters the cells.

To investigate this further, alexa-dextran 680 (emission λ = 680 μm, red, referred to as "alexa-dextran") was added to the calcein solution in which the larvae grew. Alexa-dextran has no specific binding to Ca, but being a large molecule (3,000 molecular weight) it

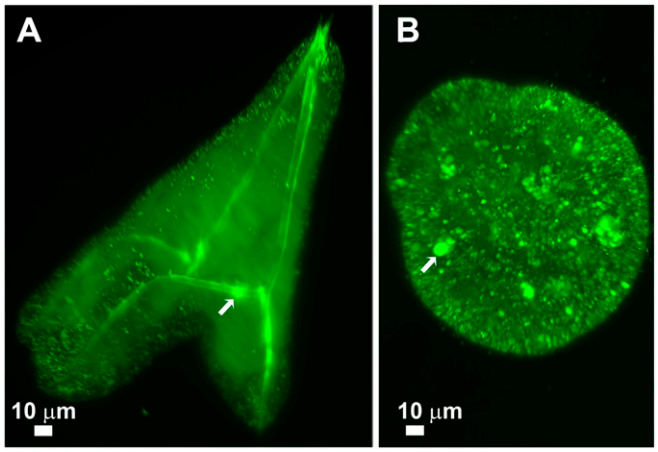

Fig. 2. Lightsheet microscope images showing a 3D reconstruction of the calcein fluorescence signal obtained from whole live larvae at the prism stage. The larvae were continuously developed inside calcein-labeled sea water from fertilization. (*A*) The control larva contains calcein-labeled particles of sizes 0.5–1 μm. The spicule is also labeled with calcein, and the center of the initial triradiate spicule (arrow) is labeled with higher fluorescence intensity compared with the spicule rods. (*B*) A larva continuously developed inside calcein-labeled sea water containing verapamil, which inhibits the functioning of L-type calcium channels. The larva is spherical and is packed with calcein-labeled particles of sizes 1–2 μm. The larger body marked with an arrow is most likely a poorly developed spicule.

too cannot penetrate into the cell through the membrane. Both calcein and alexa-dextran entered the blastocoel in a cloud-like dispersed form, and both were present as small particles inside the cells (Fig. 3 *A*–*C*). Calcein and alexa-dextran mostly colocalize in intracellular particles inside the ectoderm cells and PMCs. However, the endoderm cells contain mainly alexa-dextran–labeled particles, whereas in the PMCs many particles are only labeled by calcein (Figs. 3 *D*–*F* and 4). The spicules are labeled with calcein, but the alexa-dextran is barely present in the spicule compartment (Fig. 3*E*, *Inset*). Because the sea water is originally labeled with both calcein and alexa-dextran, the fact that particles in different tissues are differentially labeled implies an active cellular involvement in transport. Because it was specifically demonstrated in sea urchin larvae that calcein indeed tracks calcium (24, 25), and alexa-dextran tracks the transfer of sea water, we infer that the particles in the PMCs and the ectoderm derived at least some of their calcium from sea water. In contrast, the endoderm cells form particles from sea water, but without high concentrations of calcium. Random colocalization of the calcein and alexa-dextran particles was calculated and compared with the automatically measured colocalization (*SI Materials and Methods*) to verify the significance of the observations. We found that for the ectoderm cells random colocalization would result in ∼10% of the alexa-dextran and calcein being superimposed, whereas the observed colocalization is 94%. For the endoderm cells, the calculated random colocalization would be ∼10% and the observed colocalization is 26.6%, and for PMCs the calculated random colocalization would be ∼5% and the observed colocalization is 52.5% (Fig. 4).

To better understand how the labeled molecules enter the cells, and how the different distributions of labels in the three tissue types may be related to the mineralization pathway, the cellular environment of the PMCs in the vicinity of the forming spicule was characterized at high resolution and in 3D. The recently developed cryo-FIB-SEM (25, 34–36) was used to image relatively large (2,640 μm^3) volumes of high-pressure frozen prism-stage larvae close to their native state, with minimal damage due to sample preparation. Movie S1 shows part of the FIB-SEM slices in a serial manner, and Movie S2 includes the segmentation of some key features in the stack. These 3D analyses provide details of the cells and their constituent organelles and nuclei in the vicinity of the spicule, and most significantly show that the PMCs contain vesicles that have an opening through the cell plasma membrane (Fig. 5). These vesicles are thus able to exchange contents with the fluid in the blastocoel. The contents of some of these vesicles are similar in appearance to the cytoplasm (Fig. 5 *A*–*D*), that is, they show no contrast ("smooth"). Other vesicles contain dark nanoparticles dispersed inside a material having the same gray level as the cytoplasm (Fig. 5 *E* and *F*). The particles have gray levels similar to those of lipids and of proteins, which in cryo-FIB-SEM have high contrast relative to the water-rich environment of the aqueous cytosol (37). We emphasize that only 3D information can determine whether vesicles really have no contact with the membrane. Fig. 5*D* shows a vesicle with wider opening to the blastocoel, and with no neck-like structure. This vesicle is branched and not spherical. From analysis of 220 intracellular vesicles inside PMCs we determined that the majority of the intracellular vesicles have no contact with the plasma membrane. Out of 40 observed vesicles contacting the plasma membrane 13 had an opening.

To better characterize the intracellular vesicles that are open to the blastocoel, their shapes were examined by 3D segmentation of serial cryo-FIB-SEM images (Movie S2 and Fig. 6). Surprisingly, the seemingly spherical vesicles have much more complicated shapes than what was estimated from individual sections. Several vesicles that appeared isolated in individual images are actually interconnected, forming a large branched structure in 3D (segmented in Movie S2). This structure extends all of the way from the plasma membrane to the nuclear envelope (Fig. 6 *B* and *C* and Movie S2).

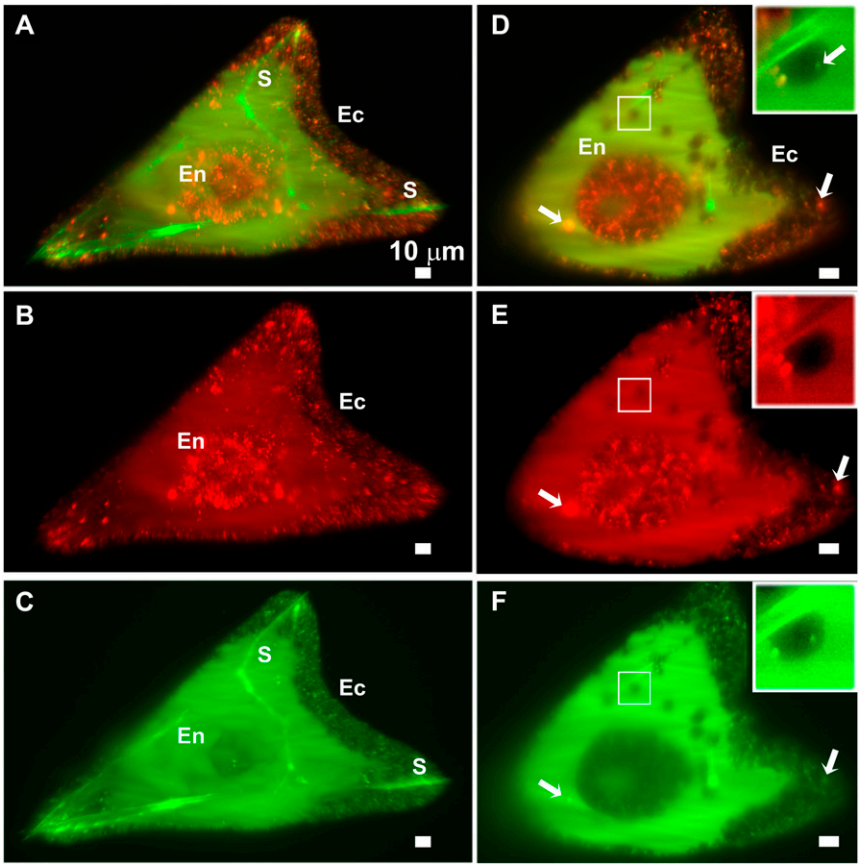

Fig. 3. Lightsheet microscope images showing calcein (green) and alexa-dextran 680 (red) fluorescence from a live larva at the prism stage. The larva was continuously developed in calcein- and dextran-Alexa 680–labeled sea water from fertilization. (*A*–*C*) Three-dimensional reconstructions of serial sections through the entire larva. (*D*–*F*) Individual slice showing the fluorescence from one plane. (*Insets*) PMC that is adjacent to the spicule (marked with a rectangle) and in focus (inset dimensions: 11 × 11 μm). (*A*) Superimposition of calcein (green) and alexa-dextran (red) fluorescence signals.The spicule is labeled with calcein. Most of the red and green labels in the larva colocalize, resulting in an orange signal, except in the spicules and in the endoderm (the gut) area. (*B*) Alexa-dextran fluorescence signal showing intracellular particles that are very prominent in the endoderm. (*C*) Calcein fluorescence signal showing the labeled spicules, intracellular calcein-labeled particles, and a cloud in the blastocoel. (*D*) Superimposition of the calcein (green) and alexa-dextran (red) fluorescence signals in one plane within the larva. Most of the particle signals colocalize (orange), but not all (arrow, compare with *E* and *F*). (*Inset*) Intracellular particles inside the PMC. (*E*) Alexa-dextran fluorescence signal. (*F*) Calcein fluorescence signal. (*D*–*F*, *Insets*) A particle that is only labeled with calcein is marked with an arrow. Ec, ectoderm cells; En, endoderm cells; and S, spicule. (Scale bars: 10 μm.)

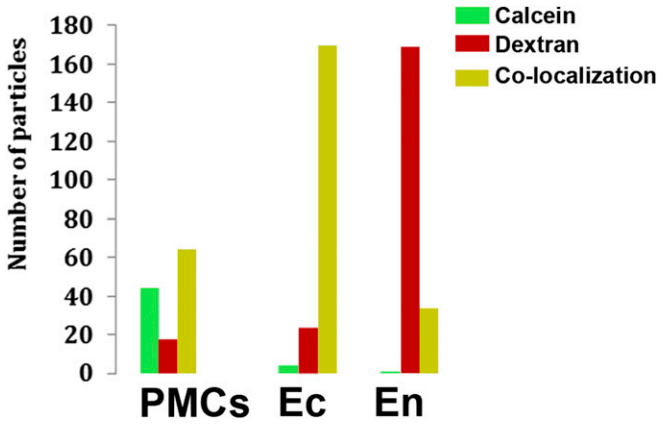

Fig. 4. The size, type of labeling, and location of 522 particles, obtained from analysis of individual Lightsheet images (*Materials and Methods*), similar to the slices shown in Fig. 3 *D–F*. The green columns represent particles that are only labeled with calcein. The red columns represent particles that are only labeled with alexa-dextran. The yellow columns represent particles in which calcein and alexa-dextran labels colocalize. Approximately half of the particles in the PMCs display label colocalization. Almost all of the particles that are located inside ectoderm cells (Ec) display label colocalization. Most of the particles that are located inside endoderm cells (En) only display alexa-dextran labeling.

Discussion

Here we show that the calcium pathway from the blastocoel to intracellular mineral particles (based on refs. 24 and 25), and finally to the spicule, involves both L-type calcium channels in membranes and a direct pathway. More detailed investigation of the direct pathway using the two fluorescent molecules, calcein and alexa-dextran dissolved in sea water, shows that the PMCs and the ectoderm cells predominantly incorporate sea water (nonspecifically labeled by alexa-dextran) and calcein that is bound to calcium. Cryo-FIB-SEM serial imaging and reconstruction show that a possible mode of incorporation of the two labeled molecules and the accompanying sea water is by exchange of the labeled sea water in the blastocoel with vesicles in the PMCs. We conclude that these independent lines of evidence support the notion that modified sea water is incorporated into the PMCs by endocytosis. A schematic representation of possible scenarios is given in Fig. 7. The characteristics of this sea water are not, as yet, known.

It is interesting to note that the endoderm cells in these experiments have particles that are labeled mainly with alexa-dextran. The proportion of particles with colocalized labels in the endoderm is much less than in the PMCs and the ectoderm cells. We assume that the earlier observations of calcein uptake into the endoderm (24) documented only the minor particle component that took up calcein. This differential labeling shows that somewhere along the pathway between the blastocoel and the formation of labeled particles calcein, and presumably its associated calcium, were discriminated against. The opposite can be concluded for spicule formation, namely that the sea water label, alexa-dextran, which was incorporated into the PMCs, was somehow excluded when the calcium was translocated to the spicule.

It is also interesting to note that blocking the activity of the L-type channels did prevent the formation of normal spicules as was previously reported (23, 26) but did not prevent the formation of the initial mineral deposits at the core of the triradiate spicules, and in some cases rudimentary triradiate spicules also formed. This means that L-type channels are not essential for initial mineral deposition, but only for the further growth of the spicule.

In the cryo-FIB-SEM observations two types of vesicles in the PMCs that form openings with the blastocoel were noted: large convoluted vesicles and smaller spherical vesicles. The convoluted branched type is reminiscent of macropinosomes associated with macropinocytosis. During macropinocytosis extracellular fluids are nonspecifically introduced into the cell (38) through relatively large and branched vacuoles, the macropinosomes (20, 39). Because most of the current studies on macropinocytosis were carried out using cell cultures, many stages of macropinocytosis in whole organisms and in vivo and their relevance to physiological processes are not yet clear (39). In the PMCs, these large convoluted vesicles may function as open spaces for incorporating relatively large amounts of sea water.

The small rounded vesicles that form openings toward the blastocoel may function in the "kiss-and-run" mode (40, 41). In kiss-and-run fusion, intracellular vesicles dock at the plasma membrane but do not fully fuse with it. At their docking location, the vesicles open and close. In this way they empty their contents into the extracellular space, and pick up new cargo from the extracellular space (42). Elevation in extracellular calcium concentration induces kiss-and-run fusion (43, 44). Thus, in the context of the PMCs, these vesicles may actively transport sea water to specific locations inside the cell.

There is one well-documented case of sea water endocytosis in the field of biomineralization, namely in certain unicellular foraminifera that form calcitic shells (2). The foraminifera also incorporate fluorescently labeled dextran and calcein into large convoluted vacuoles inside their cytoplasm, showing that they are taking up sea water by endocytosis (2). These sea water vacuoles can also be imaged using back-scattered detection on cryo-fixed specimens observed in the SEM where they have the same contrast as sea water (45). Furthermore, the foraminifera also concentrate their calcein label in small rounded vesicles and the label eventually reaches the shell (2, 45). The observed pathways in the foraminifera and the sea urchin are therefore in many respects analogous. This observation raises the possibility that other marine organisms, both single-celled and multicelled, may also exploit the endocytosis mechanism to incorporate sea water for the purpose of transporting calcium and probably carbonate or phosphate to the site of mineralization.

Conclusions

Calcium uptake from the blastocoel fluid, which is essentially sea water, occurs by at least two pathways. One pathway involves L-type calcium channels and these are involved in spicule

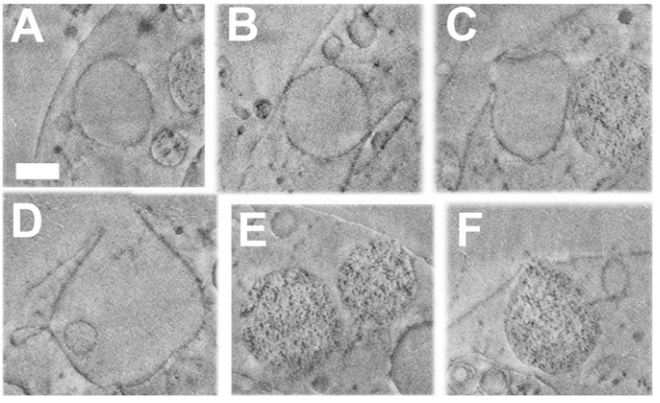

Fig. 5. Cryo-FIB-SEM micrographs of parts of a PMC from a sea urchin larva at the prism stage. Proteins, lipids, and membranes appear dark, whereas water-rich regions such as aqueous cytosol appear in uniform light gray in cryo-FIB-SEM. The series of micrographs is taken from Movie S1. (*A–D*) Vesicles bearing a uniform content similar in texture and gray levels to cytoplasm and extracellular fluids. (*E* and *F*) Vesicles containing dark particles. (*A*) No contact of the vesicle with the plasma membrane. (*B*) The vesicle contacts the plasma membrane. (*C*) The vesicle is open toward the blastocoel. (*D*) The vesicle has a wide opening toward the blastocoel and branches into smaller vesicles. (*E*) One vesicle (to the right) touches the plasma membrane, but the other does not. (*F*) Vesicle in contact with the plasma membrane and open toward the blastocoel. (Scale bars: 500 nm for all panels.)

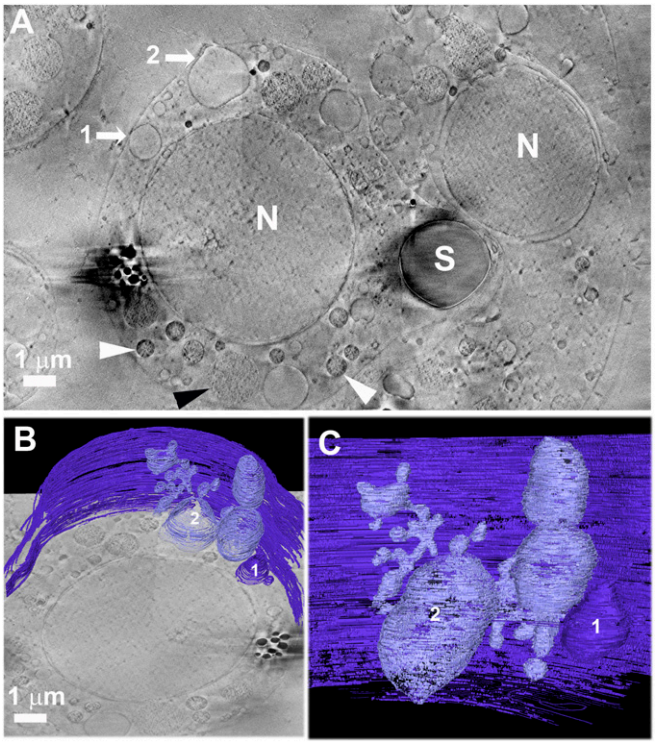

Fig. 6. (*A*) Cryo-FIB-SEM micrograph of a single section of a high-pressure-frozen sea urchin larva at the prism stage, taken from Movie S1. Vesicles that are in contact with the plasma membrane of a PMC are marked by arrows, 1 and 2. The vesicle labeled "2" is the same as in Fig. 5*D* but taken from a different section. Organelles such as mitochondria are detected (white arrowhead), as well as nanoparticle-containing vesicles (black arrowhead). The black organelles on the left of the picture are most probably lipid bodies. (*B* and *C*) Three-dimensional manual segmentation of the plasma membrane and the vesicles that are in contact with it. The 3D view reveals that vesicles (1 and 2) are connected to each other, forming a branched 3D intracellular vacuole with multiple docking points in the plasma membrane. The vacuole spreads and in some locations is in close proximity to the nuclear envelope. See also Movie S2. N, nuclei and S, spicule. Contrast differences between the two sides of the image result from image processing (see Methods).

formation. The second pathway involves calcium entering the tissues without passing through membranes. Double labeling with the membrane-impermeable markers calcein and the large fluorescent molecule alexa-dextran shows that both labels are present in particles in the PMCs and ectoderm cells, but calcein is largely excluded from endoderm cells and concentrated in the spicule. Cryo-FIB-SEM serial imaging identifies the presence in PMCs of intracellular vesicles that form small openings through the plasma membrane to the blastocoel. We infer from all these observations that some calcium is actively transported through calcium channels into the tissues and ultimately to the spicule, but in addition calcium is transported passively by sea water being taken up into vesicles inside the PMCs. Cellular processing of the sea water somehow results in calcium being concentrated in what are most likely intracellular particles in the ectoderm and the PMCs. Cellular processing in the endoderm, for the most part, excludes calcium entering the particles. The inferred sea water uptake process in sea urchin larvae is reminiscent of the manner in which foraminifera form their calcitic shells by endocytosing sea water.

Materials and Methods

Sea Urchin Larval Culture. Mature cultured adult sea urchins *Paracentrotus lividus* were supplied by the Israel Oceanographic and Limnological Research Institute. Spawning, fertilization, and embryo development were carried out as described (25). When the prism (46) developmental stage was reached, the samples were imaged in vivo or high-pressure-frozen without any processing, as described below. The research involving sea urchins is approved by the Israel Oceanographic and Limnological Research, National Center for Mariculture.

Calcium Channel Inhibition. Verapamil HCl (V4629; Sigma-Aldrich), 100 μM, was dissolved in double-distilled water. Fifty microliters of verapamil were transferred into 5 mL sea urchin larva suspension after fertilization. This concentration was based on the results of testing a series of verapamil concentrations as assessed both by the spicule morphology and the larvae's general appearance compared with control larvae. We then chose the verapamil concentration in which the larvae had morphologies similar to those of the control larvae, yet their spicule development was inhibited. Higher verapamil concentrations induced changes in the general larva appearance.

Fluorescence Labeling. Calcein, 20 μM (154071484; Sigma-Aldrich), was dissolved in sea water containing 30 mg/L penicillin G sodium salt (69578; Sigma-Aldrich) and 15 mg/L streptomycin sulfate salt (3810740; Sigma-Aldrich) and filtered in a 0.22-μm sterile Corning filter system. Dextran-Alexa Fluor 680 3,000 molecular weight (D-34681; Life Technologies), 50 μM, was dissolved in seawater. For labeling, developing larvae were immersed from fertilization in calcein- or dextran-alexa–labeled sea water at 18 °C with gentle shaking (100 rpm). At the prism or pluteus stage the larvae were washed with sea water and examined.

Sample Mounting for Microscopy Experiments. One microliter of the larvae suspension was quickly introduced into 60 μL of 4% (wt/vol) Agarose Low Melt (9012-36-6; Carl Roth) inside sea water. A droplet of the larva–agarose mixture was quickly transferred onto a glass slide and was covered with a glass coverslip for optical and polarized light imaging.

Polarized Light Imaging. Optical images were taken using a Nikon microscope (Eclipse E600 Pol), with or without polarizers in cross position.

SPIM Imaging. One microliter of the larva suspension was quickly placed inside 60 μL of 4% (wt/vol) Agarose Low Melt (9012-36-6; Carl Roth) dissolved inside sea water. The larva–agarose mixture was gently loaded into a 10-μL

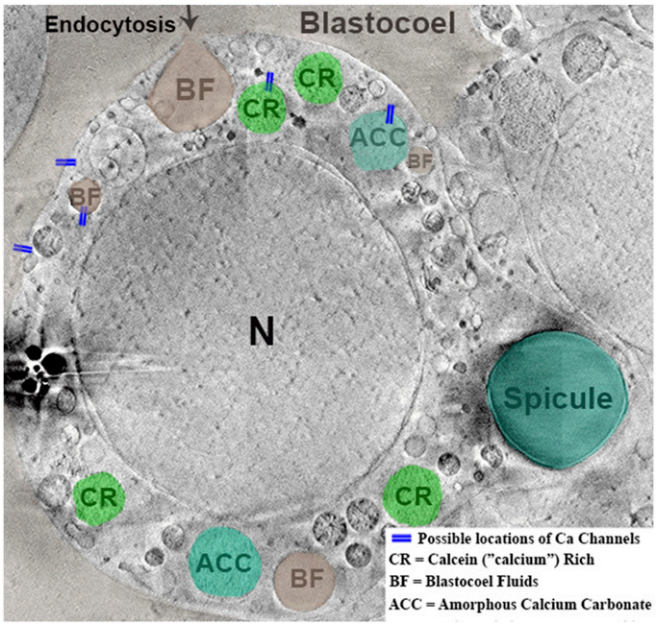

Fig. 7. Schematic representation of the conceivable scenarios for the endocytosis process, overlaid on a cryo-FIB-SEM micrograph. Colors were arbitrarily designated to the intracellular vesicles to show possible cellular processing of the uptaken blastocoel fluids (BF). Possible location of calcein-rich (CR) and amorphous calcium carbonate (ACC) vesicles are shown in green. The blue lines indicate some of the possible locations of calcium channels in the cells and vesicles. Contrast differences between the two sides of the image result from image processing (see Methods).

glass capillary (BR-7019-02; Brand GMBH) in a syringe-like mode. After the gel solidified, the sample (in the gel "rod") was pushed outside the capillary into the microscope chamber, which was filled with sea water.

The fluorescence images were obtained using a Lightsheet Z.1 microscope (Carl Zeiss Microscopy GmbH) with a 20× water objective. Calcein was excited at 488 nm and the emission was collected with a BD 505- to 545-nm filter. Dextran-alexa 680 was excited at 638 nm and the emission was separated using an LP 660-nm filter. The laser intensities were 5% for calcein and 4% for dextran-alexa 680. The exposure time was 99.9 ms, with a voxel size of $0.152 \times 0.152 \times 0.469$ μm. The total number of slices acquired in the *z* axis for each larva was for Fig. 2*A* 352 slices, Fig. 2*B* 293 slices, and Fig. 3 333 slices. Three-dimensional reconstruction of the slices was performed using Imaris 8.2 (Bitplane; Oxford Instruments).

Sample Preparation for Cryo-Imaging. Larvae at the prism or pluteus stage were high-pressure-frozen: 10 μL of the larva suspension inside 10% (wt/vol) dextran in sea water were sandwiched between two metal discs (3-mm diameter and 0.1-mm and 0.05-mm cavities) and cryo-immobilized in a high-pressure-freezing device (HPM10; Bal-Tec).

Cryo-FIB-SEM 3D Imaging. Cryo-FIB-SEM of native high-pressure-frozen sea urchin larvae at the prism stage was carried out using an Auriga 60 FIB-SEM (Carl Zeiss Microscopy GmbH). Throughout the imaging the samples were kept below −145 °C. Slices of the sample were removed by FIB milling in a serial manner using an FIB probe current of 600 pA, and each of the freshly exposed cross-sections was observed by SEM imaging at 1.8 kV using InLens SE detection. Voxel sizes (image pixel size in X direction × image pixel size in Y direction × slice thickness) used in this study were $10 \times 10 \times 20$ nm.

Image Analysis. The obtained images were aligned using ImageJ (NIH) and Avizo 9 software (FEI). Noise filtering, including elimination of curtaining, was carried out by using the ImageJ software through FFT-based corrections. Contrast enhancement was obtained with the "enhance contrast" process of ImageJ applied to the entire stack of the FIB-SEM data. In order to process such a large dataset, we cut the original block into smaller blocks. We then automatically enhanced the contrast of the smaller blocks from the Y direction (one YZ slice at a time) and merged all the images into the original block. Since contrast enhancing was done automatically, contrast differences appear on the XY plane, where the separate blocks meet. Three-dimensional reconstruction was done with Avizo. Segmentation was carried out manually by the "magic wand" tool in Avizo. After smoothing, isosurfaces were generated from the segmented data. Brightness, contrast, and gray levels of single images were adjusted by Adobe Photoshop CS 4 Extended (Adobe Systems).

ACKNOWLEDGMENTS. We thank Neta Varsano and Moshe Varsano for their help with colocalization calculations, Allon Weiner for discussions on endocytosis and for segmentation tips, and Maria Pierantoni and Ofra Golani for help with Avizo and Imaris software. The research was supported by a German Research Foundation grant within the framework of the Deutsch–Israelische Projektkooperation and Department of Energy Award DE-FG02-07ER15899. L.A. is the incumbent of the Dorothy and Patrick Gorman Professorial Chair of Biological Ultrastructure, and S.W. is the incumbent of the Dr. Trude Burchardt Professorial Chair of Structural Biology.

1. Guéguen L, Pointillart A (2000) The bioavailability of dietary calcium. *J Am Coll Nutr* 19(sup2):119S–136S.
2. Bentov S, Brownlee C, Erez J (2009) The role of seawater endocytosis in the biomineralization process in calcareous foraminifera. *Proc Natl Acad Sci USA* 106(51):21500–21504.
3. Nakano E, Okazaki K, Iwamatsu T (1963) Accumulation of radioactive calcium in larvae of the sea urchin *Pseudocentrotus depressus*. *Biol Bull* 125(1):125–132.
4. McMahon RF, Bogan A (1991) *Mollusca: Bivalvia. Ecology and Classification of North American Freshwater Invertebrates*, eds Thorp JH, Covich AP (Academic, San Diego), pp 315–399.
5. Young JR, Henriksen K (2003) Biomineralization within vesicles: The calcite of coccoliths. *Rev Mineral Geochem* 54(1):189–215.
6. Weiner S, Addadi L (2011) Crystallization pathways in biomineralization. *Annu Rev Mater Res* 41:21–40.
7. Tambutté S, et al. (2011) Coral biomineralization: From the gene to the environment. *J Exp Mar Biol Ecol* 408(1):58–78.
8. Tambutté E, et al. (2012) Calcein labelling and electrophysiology: Insights on coral tissue permeability and calcification. *Proc Biol Sci* 279(1726):19–27.
9. Kerschnitzki M, et al. (2016) Transport of membrane-bound mineral particles in blood vessels during chicken embryonic bone development. *Bone* 83:65–72.
10. Beniash E, Addadi L, Weiner S (1999) Cellular control over spicule formation in sea urchin embryos: A structural approach. *J Struct Biol* 125(1):50–62.
11. Boonrungsiman S, et al. (2012) The role of intracellular calcium phosphate in osteoblast-mediated bone apatite formation. *Proc Natl Acad Sci USA* 109(35):14170–14175.
12. Couradeau E, et al. (2012) An early-branching microbialite cyanobacterium forms intracellular carbonates. *Science* 336(6080):459–462.
13. Kerschnitzki M, et al. (2016) Bone mineralization pathways during the rapid growth of embryonic chicken long bones. *J Struct Biol* 195(1):82–92.
14. Mahamid J, et al. (2010) Mapping amorphous calcium phosphate transformation into crystalline mineral from the cell to the bone in zebrafish fin rays. *Proc Natl Acad Sci USA* 107(14):6316–6321.
15. Brown BE (1982) The form and function of metal-containing 'granules' in invertebrate tissues. *Biol Rev Camb Philos Soc* 57(4):621–667.
16. Berridge MJ, Taylor C (1988) Inositol trisphosphate and calcium signaling. *Cold Spring Harbor Symp Quant Biol* 53:927–933.
17. Bauer W, Aub JC, Albright F (1929) Studies of calcium and phosphorus metabolism: V. a Study of the bone trabeculae as a readily available reserve supply of calcium. *J Exp Med* 49(1):145–162.
18. Albers RW (1967) Biochemical aspects of active transport. *Annu Rev Biochem* 36(1):727–756.
19. de Meis L, Vianna AL (1979) Energy interconversion by the Ca^{2+}-dependent ATPase of the sarcoplasmic reticulum. *Annu Rev Biochem* 48(1):275–292.
20. Mayor S, Pagano RE (2007) Pathways of clathrin-independent endocytosis. *Nat Rev Mol Cell Biol* 8(8):603–612.
21. Stumpp M, et al. (2012) Acidified seawater impacts sea urchin larvae pH regulatory systems relevant for calcification. *Proc Natl Acad Sci USA* 109(44):18192–18197.
22. Guss KA, Ettensohn CA (1997) Skeletal morphogenesis in the sea urchin embryo: Regulation of primary mesenchyme gene expression and skeletal rod growth by ectoderm-derived cues. *Development* 124(10):1899–1908.
23. Hwang S-PL, Lennarz WJ (1993) Studies on the cellular pathway involved in assembly of the embryonic sea urchin spicule. *Exp Cell Res* 205(2):383–387.
24. Vidavsky N, et al. (2014) Initial stages of calcium uptake and mineral deposition in sea urchin embryos. *Proc Natl Acad Sci USA* 111(1):39–44.
25. Vidavsky N, Masic A, Schertel A, Weiner S, Addadi L (2015) Mineral-bearing vesicle transport in sea urchin embryos. *J Struct Biol* 192(3):358–365.
26. Yasumasu I, Mitsunaga K, Fujino Y (1985) Mechanism for electrosilent Ca^{2+} transport to cause calcification of spicules in sea urchin embryos. *Exp Cell Res* 159(1):80–90.
27. Mitsunaga K, Makihara R, Fujino Y, Yasumasu I (1986) Inhibitory effects of ethacrynic acid, furosemide, and nifedipine on the calcification of spicules in cultures of micromeres isolated from sea-urchin eggs. *Differentiation* 30(3):197–204.
28. Wilt FH (2002) Biomineralization of the spicules of sea urchin embryos. *Zoolog Sci* 19(3):253–261.
29. Wilt FH, Killian CE, Hamilton P, Croker L (2008) The dynamics of secretion during sea urchin embryonic skeleton formation. *Exp Cell Res* 314(8):1744–1752.
30. Ehara T, Daufmann R (1978) The voltage- and time-dependent effects of (-)-verapamil on the slow inward current in isolated cat ventricular myocardium. *J Pharmacol Exp Ther* 207(1):49–55.
31. Kohlhardt M, Bauer B, Krause H, Fleckenstein A (1972) Differentiation of the transmembrane Na and Ca channels in mammalian cardiac fibres by the use of specific inhibitors. *Pflugers Arch* 335(4):309–322.
32. Tytgat J, Vereecke J, Carmeliet E (1988) Differential effects of verapamil and flunarizine on cardiac L-type and T-type Ca channels. *Naunyn Schmiedebergs Arch Pharmacol* 337(6):690–692.
33. Fujino Y, Mitsunaga K, Fujiwara A, Yasumasu I (1985) Inhibition of $^{45}Ca^{2+}$ uptake in the eggs and embryos of the sea urchin, *Anthocidaris crassispina*, by several calcium antagonists, anion transport inhibitor, and chloride transport inhibitors. *J Exp Zool* 235(2):281–288.
34. Sviben S, et al. (2016) A vacuole-like compartment concentrates a disordered calcium phase in a key coccolithophorid alga. *Nat Commun* 7:11228.
35. Schertel A, et al. (2013) Cryo FIB-SEM: Volume imaging of cellular ultrastructure in native frozen specimens. *J Struct Biol* 184(2):355–360.
36. Bennet M, et al. (2015) Biologically controlled synthesis and assembly of magnetite nanoparticles. *Faraday Discuss* 181:71–83.
37. Vidavsky N, et al. (September 28, 2016) Cryo-FIB-SEM serial milling and block face imaging: Large volume structural analysis of biological tissues preserved close to their native state. *J Struct Biol*, 10.1016/j.jsb.2016.09.016.
38. Doherty GJ, McMahon HT (2009) Mechanisms of endocytosis. *Annu Rev Biochem* 78: 857–902.
39. Lim JP, Gleeson PA (2011) Macropinocytosis: An endocytic pathway for internalising large gulps. *Immunol Cell Biol* 89(8):836–843.
40. Ceccarelli B, Hurlbut WP, Mauro A (1973) Turnover of transmitter and synaptic vesicles at the frog neuromuscular junction. *J Cell Biol* 57(2):499–524.
41. Del Castillo J, Katz B (1954) Quantal components of the end-plate potential. *J Physiol* 124(3):560–573.
42. Harata NC, Aravanis AM, Tsien RW (2006) Kiss-and-run and full-collapse fusion as modes of exo-endocytosis in neurosecretion. *J Neurochem* 97(6):1546–1570.
43. Alés E, et al. (1999) High calcium concentrations shift the mode of exocytosis to the kiss-and-run mechanism. *Nat Cell Biol* 1(1):40–44.
44. Elhamdani A, Azizi F, Artalejo CR (2006) Double patch clamp reveals that transient fusion (kiss-and-run) is a major mechanism of secretion in calf adrenal chromaffin cells: High calcium shifts the mechanism from kiss-and-run to complete fusion. *J Neurosci* 26(11):3030–3036.
45. Khalifa GM, et al. (2016) Biomineralization pathways in a foraminifer revealed using a novel correlative cryo-fluorescence-SEM-EDS technique. *J Struct Biol* S1047-8477(16)30014-4.
46. Giudice G (2012) *Developmental Biology of the Sea Urchin Embryo* (Elsevier, New York).